# Self-Assembled Networks of Ribbons in Molecular Hydrogels of Cationic Deoxycholic Acid Analogues

**Pierre Terech,*,† Neralagatta M. Sangeetha,‡ Bruno Demé,§ and Uday Maitra‡**

*UMR5819, CEA-CNRS, Université J. Fourier, DRFMC-SI3M, CEA-Grenoble, 17 rue des Martyrs, 38054 Grenoble, Cedex 9, France, Department of Organic Chemistry, Indian Institute of Science, Bangalore 560 012, India, and Institut Laue Langevin, 6 rue Jules Horowitz, BP 156, 38042 Grenoble, Cedex 9, France*

*Received: February 7, 2005; In Final Form: May 9, 2005*

Aqueous gels derived from three cationic 24-*nor* 3,12-dihydroxy cholane (DC) derivatives with *N*-methyl-2-pyrrolidinone (NMP), *N*-methylmorpholine (NMM), and 1,4-diazabicyclo[2.2.2]octane (DABCO) at the side chain positions have been exhaustively characterized by small-angle neutron-scattering experiments. Although the molecular structures differ slightly by the heterocycle grafted to the steroid core, the derived gels exhibit a range of structural behaviors at the nanoscale that depart from those observed with simple deoxycholate systems. The NMM-DC aggregates are ribbons with a bimolecular thickness of $t = 37$ Å and an anisotropy of the section $b/a \approx 0.1$. DABCO-DC exhibits a remarkable transition from ribbons ($t = 29.5$ Å, $b/a = 0.18$) to thicker cylindrical fibers ($R \approx 59$ Å), involving four original ribbons, upon a concentration increase. The NMP-DC system forms thick cylindrical fibers ($R \approx 68$ Å) with steroid molecules organized in a specific morphology. Bilayered or interdigited structures are formed and favored by the presence of multiple polar interaction centers in the DC molecules. Secondary aggregation mechanisms are invoked in the formation of bundles having a lower cross-sectional anisotropic symmetry and exhibiting Bragg peaks corresponding to molecular length periodicities. The relations between the structural information and the rheological properties are discussed.

## Introduction

The application potentials of supramolecular gels have evoked a great interest in these materials and triggered much activity in the studies pertaining to their structure and function in the recent years. These soft solidlike materials formed by the spontaneous self-assembly of low-mass molecules to yield fibrillar networks can entrap large amounts of liquids. Although the first of the reports on such systems appeared in the early 19th century, for instance, gelation of aqueous solutions by lithium urate was reported as early as 1841,[1] they remained neglected until the late 20th century. A renewal in interest in the exploration of these materials is due to the emergence of powerful techniques, such as scattering methods using high-flux sources and microscopic techniques. The simplicity of preparation of supramolecular gels, the thermal reversibility of their viscoelastic properties at moderate temperatures (<100 °C), and the well-defined rodlike structures forming the networks are favorable attributes that have motivated the fundamental and applied research efforts dedicated to them.[2] Studies on structural aspects of these heterogeneous materials have been a challenge guided by the pursuit to link the "chemical structures" of the basic monomeric units through the nanoscale-length structures of the self-assembled fibrillar networks (SAFINs) to the final macroscopic properties.

The present work details small-angle neutron scattering (SANS) investigations on three cationic 24-*nor* 3,12-dihydroxy cholane (DC)-derived hydrogels (*N*-methyl-2-pyrrolidinone-DC (NMP-DC), *N*-methylmorpholine-DC (NMM-DC), and 1,4-diazabicyclo[2.2.2]octane-DC (DABCO-DC)) previously investigated[3] by us. The SANS technique explores the structures in the 10 to 6000 Å range using scattering curves over almost three angular decades in the reciprocal space. The three compounds differ in the nature of the heterocycle grafted to the steroid platform (Chart 1). It appears that the moderate differences in the chemical structures have a significant effect on the aggregation behaviors. Hydrogels derived from these three derivatives show a diversity of properties on molecular, microscopic, and macroscopic scales. Scanning electron micrographs characterized the corresponding xerogels made up of entangled rigid fibers. The comparison of the flowing properties has underlined the singular situation of NMM-DC gels. The exponents of the scaling of the rheological parameters with the concentration for NMP-DC and DABCO-DC agreed well with those expected for cellular solids or strongly interacting colloidal gels. Conversely, the NMM-DC system exhibited a remarkable behavior with the energy of interaction between the colloidal flocs increasing with the concentration. Considering that these scaling exponents are an indication of the way the elasticity of a basic unit (i.e., floc or cell) is transduced through the macroscopic network, it is interesting to compare now the structural properties of the three DC gels.

In the search for distinctive structural properties of the gels, different length scales can be considered. The molecular scale has already been approached with crystallographic data and has shown differences in the packing modes of the cationic gelators and their morphology's modifications in gelling or nongelling conditions. Herein, we endeavor to complete the description of the DC-fibrillar networks by structural investigations at the

* Author to whom correspondence should be addressed. Phone: +33 (0)4 38 78 59 98. Fax: +33 4 38 78 56 91. E-mail: pterech@cea.fr.
† CEA-Grenoble.
‡ Indian Institute of Science.
§ Institut Laue Langevin.

10.1021/jp050666l CCC: $30.25 
Published on Web 06/04/2005

**CHART 1: DC Molecules with Average Molecular Lengths of ≈17 Å**

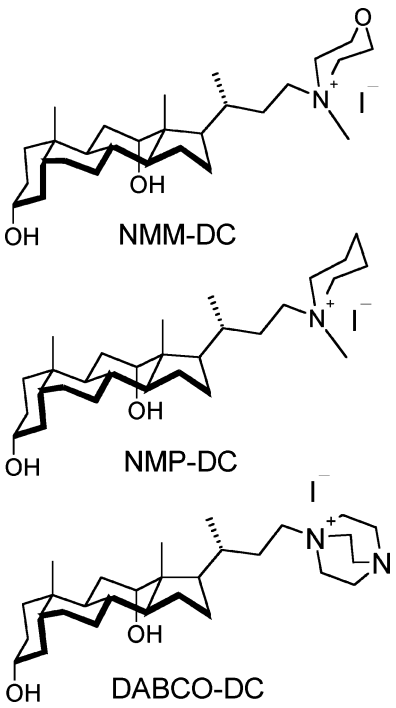


nanoscopic scale. The three DC gels exhibit distinct scattering properties whose sensitivity to concentration is unequivocal. Also, the existence of ribbonlike fibers in the network is incidental, and the work is a rare example of their structural characterization by scattering measurements. It illustrates the versatility of the steroid platform already known to produce spherical micelles, vesicles,[4] helical fibrils, and tubules.[5]

## Experimental and Methods

The synthesis of the gelators, NMP-DC ($C_{29}H_{52}NO_2I$, $d$ = 1.1), NMM-DC ($C_{28}H_{50}NO_3I$, $d$ = 1.35), and DABCO-DC ($C_{29}H_{51}N_2O_2I$), has been described elsewhere.[3] Gels were prepared in Suprasil Quartz cells of a 1-mm path by gentle heating of the gelators and $D_2O$ or electrolyte solutions and cooling naturally to room temperature.

Scattering data were obtained at the European neutron facility, Institut Laue Langevin (Grenoble, France), using the D22 spectrometer[6] at three distances (1.5, 14.4, and 17.6 m) and two wavelengths (6 and 15 Å), the detector being centered or translated by 0.25 m (at 1.5 and 14.4 m distances). The corresponding momentum transfer range was 0.6 $Å^{-1} < Q <$ 0.001 $Å^{-1}$ with $Q = 4\pi/\lambda \sin\theta$, $\lambda$ being the neutron wavelength and $\theta$ half of the scattering angle. Standard corrections and calibration procedures have been used to proceed with the radial averaging of isotropic two-dimensional arrays of neutron counts collected on the detector (128 × 128 pixels for an area of 96 × 96 $cm^2$ and a pixel size of 0.75 × 0.75 $cm^2$). Adjustment of the level of incoherent scattering (arising from all free and aggregated DC molecules) has taken advantage of $IQ^4$ versus $Q$ Porod's plots assuming sharp boundaries of the aggregates. Data analysis was made within a single-particle scattering context after a careful examination of the effect of the concentration on the scattering profiles. The specialized methodology for the analysis of the scattering from molecular gels is described elsewhere.[2] Only equations related to ribbonlike structures are summarized in the following. Details for cylindrical or ribbonlike fibers are collected in the Supporting Information. The scattering by ribbonlike structures was modeled with eq 1 ($b/a$ is the anisotropy of the elliptical section, $b$ being half of the short axis and $a$ half of the long axis).[7−9]

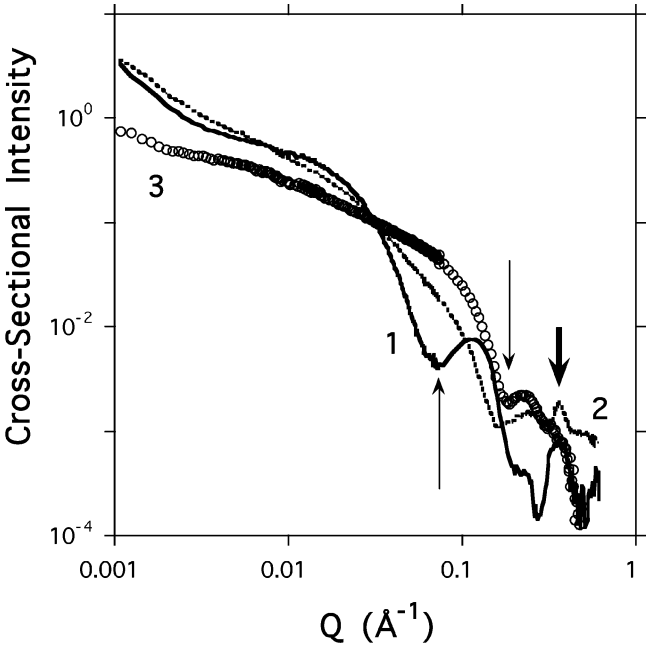


**Figure 1.** Absolute cross-sectional scattered intensity versus $Q$ curves for the three DC hydrogels in 0.5 M NaCl: 1 (full line), NMP-DC gel at $C$ = 0.00946 g $cm^{-3}$; 2 (open circles), NMM-DC gel at $C$ = 0.01052 g $cm^{-3}$; **3** (full circles), DABCO-DC gel at $C$ = 0.0172 g $cm^{-3}$.

$$QI(Q) \propto \int_0^{\pi} \left[ \frac{2J_1\left[Qa\sqrt{\left(\frac{1+(b/a)^2}{2}\right)+\left(\frac{1-(b/a)^2}{2}\right)\cos\varphi}\right]}{Qa\sqrt{\left(\frac{1+(b/a)^2}{2}\right)+\left(\frac{1-(b/a)^2}{2}\right)}} \right]^2 d\varphi \quad (1)$$

As expected for fibrillar scatterers, a ln($QI$) versus $Q^2$ plot can be used to extract their cross-sectional radii of gyration. It appears that, depending on the anisotropy ratios $b/a$ of the cross sections, the validity condition $QR_c < 1$ can be apparently not fulfilled while a reasonable straight fit is observed. Through the use of the approximation $J_1(x)/x \rightarrow {}^1/_2(1 - x^2/8)$ at $x \rightarrow 0$, the expansion of eq 1 at low $Q$ values, simplifies to

$$QI \rightarrow \pi\left[1 - \frac{Q^2a^2}{8}(1+(b/a)^2)\right] \quad (2)$$

From which a cross-sectional radius of gyration $R_c$ can be estimated

$$R_c \cong \frac{a^2+b^2}{4} \quad (3)$$

Depending upon $b/a$, the analysis can be delicate (Supporting Information) using either ln($IQ^2$) versus $Q^2$ or ln($IQ$) versus $Q^2$ plots.

## Results and Analysis

Figure 1 compares the scattering of the three DC hydrogels at similar concentrations and ionic strengths. The scattering behaviors are strikingly distinct for the three gelators while NMP-DC departs from NMM-DC and DABCO-DC. The scattering curve of the NMP-DC gel shows a broad and intense

oscillation at a much lower $Q$ value (minimum at ca. 0.078 Å$^{-1}$) than those for the two other systems (arrows in Figure 1) indicative of a larger characteristic distance. The analysis is made in the framework of fibrillar systems since the solidlike part of the molecular gels was characterized by previous scanning electron micrographs (xerogels) as densely entangled networks of fibers.[3] Characteristic scattering features[2] for unidirectional and rigid aggregates with large aspect ratios are thus expected. The major evidence should be a $Q^{-1}$ intensity decay at low angles in the limit $L$, $L_p < Q < 1/(2R)$ (with $L_p$ being the persistence length of the fibrillar aggregate, $L$ its contour length, and $R$ its radius), which was not clearly observed. SANS experiments involve the irradiation of a large volume of the specimen (typically 50 $\mu$L), and the observation integrates all structural aspects from the nanometer to the millimeter scale. Thus, all components of the SAFINs (fibers, bundles, and domains) are concerned by the Fourier transform resulting in the two-dimensional patterns. The absence of a clear $Q^{-1}$ signature with fibrillar systems can be accounted for by two reasons. First, the linear scatterers (or their bundles) can be too thick, and the experimental lowest $Q$ limit is not low enough to fulfill the observation condition. Second, the shape of the sections can be anisotropic with one of the two dimensions being too large (flat ribbons). In a $QI$ versus $Q$ representation, the $Q^{-1}$ behavior is observed as a plateaulike part usually delimited with sharper decays on both $Q$ sides. The low $Q$ decay corresponds to interferences at large distances as those produced by heterogeneities or junction zones in the SAFINs. The large $Q$ sharp decay corresponds to interferences at short distances as those produced by the sections of fibers. Figure 1 shows that, despite the overlap of the two above regions, a flattening of the decay typical of fibrillar scatterers can still be distinguished with NMP-DC. This observation will be further supported by the analysis at larger $Q$ values (known as Guinier's analysis). In conditions[10] where the inequality $2\pi/L_p < Q < \pi/R_c$ holds, linear ln($QI$) versus $Q^2$ plots are obtained with rigid rodlike scatterers from which the cross-sectional radius of gyration $R_c$ can be extracted. Figure 2 shows the three DC gels, and Table 1 collects the $R_c$ and extrapolated $(QI)_0$ values. The NMP-DC hydrogel exhibits a singular behavior with a remarkably larger value of the slope (and so $R_c$) as compared to those of NMM-DC and DABCO-DC, differing by 1 order of magnitude. The analysis now attempts to model the scattering assuming first homogeneous and cylindrical fibers with a diameter consistent with the extracted $R_c$ values.

**NMP-DC Hydrogels.** Simple structural hypotheses (e.g., homogeneous or heterogeneous cylinders) cannot reproduce the SANS curve for NMP-DC (not shown). A concentration study is used to decipher the origin of the broad oscillation at $Q =$ 0.115 Å$^{-1}$. Figure 3 shows that the curves vary significantly not only in the low $Q$ region but also in the region of the first oscillation. The Bragg peak at ca. 0.35 Å$^{-1}$ does not shift with $C$ and corresponds to the first diffraction peak ([020] planes in the orthorhombic $C222_1$ group of the regular crystalline morphology.[3] At $Q = 0.124$ Å$^{-1}$ (curve 3, Figure 3), the concentrated gel exhibits a bump apparently resulting from the composition of the first form-factor oscillation of the fibers and an underlying Bragg peak. The amount of extra scattering at the innermost part of the scattering also becomes significant, and the flattened zone ($I \approx Q^{-1}$) can no longer be discerned. The spacing corresponding to this "hidden Bragg peak" is ca. 50.7 Å and does not correspond to any diffraction feature of the gelator in its usual crystalline morph (obtained in nongelling conditions). The observation suggests that the molecules adopt

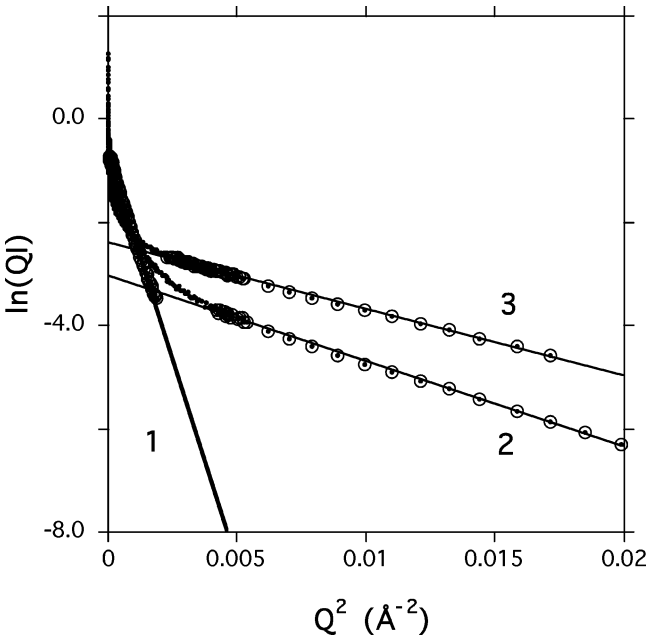


**Figure 2.** Plots of ln($QI$) versus $Q^2$ allow the extraction (Table 1) of the cross-sectional radii of gyration $R_c$ of rodlike aggregates in DC hydrogels of Figure 1: 1, NMP-DC; 2, NMM-DC; 3, DABCO-DC. Open circles with a center dot are experimental data taken for the linear fit.

a different arrangement in the fibers of the hydrogel. The scattering profile can be reproduced if a composite signal is considered (not shown), summing the form-factor contribution with an underlying Bragg peak at ca. 0.14 Å$^{-1}$. A cylindrical morphology with $R = 68$ Å is an average model that can be improved by introducing a moderate anisotropy of the sections (e.g., elliptical with $b = 58$ Å, $b/a = 0.7$). The characteristic distances involved in the models appear slightly larger than the bimolecular length, suggesting a complex aggregation mechanism.

**NMM-DC Hydrogels..** The NMM-DC system exhibits a very different scattering pattern at a similar low concentration (Figure 1). The power law of the decay is $Q^{-1.92}$ over more than one $Q$ decade (from 0.001 to 0.024 Å$^{-1}$) and departs from the expected behavior for cylindrical fibers ($I \propto Q^{-1}$). In addition, an extended linear part is identified in a Guinier plot for lamellar-like systems (Figure 4). In addition, Figure 1 also shows a well-resolved form-factor oscillation at $Q \approx 0.17$ Å$^{-1}$ accounting for the monodispersity of the transverse dimension of the fibrillar scatterers. These observations support the analysis using a ribbonlike model with a thickness $t \approx 37$ Å. The lateral extension of the rectangular section is large enough to produce an asymptotic low $Q$ decay close to $Q^{-2}$ in the limit of the experimental SANS length scale (ca. 6000 Å). A theoretical scattering profile for ribbons with elliptical sections (40 Å × 400 Å) using eq 1 reproduces the experimental pattern (Figure 5). The agreement concerns not only the asymptotic low $Q$ region but also the subsequent sharp decay and the large $Q$ oscillation as well. To the best of our knowledge, it is a rare example of a scattering characterization of ribbonlike structures that will be further complemented (vide infra). The particular profile of the ln($Q^2I$) versus $Q^2$ plot in Figure 4 also shows a low $Q$ peak at $Q^2 \approx 0.00025$ Å$^{-2}$. The peak indicates a correlation distance $\langle d \rangle$ related to the finite size of the large axis of the section. The numerical value $\langle d \rangle = 2\pi/\sqrt{0.00025} \approx$ 400 Å appears to be identical to that used for the fit of the scattering profile (Figure 5) and is an additional confirmation of the ribbon structure. At the other end of the scattering curve,

**TABLE 1: Guinier's Analysis for the Three DC Systems in 0.5 M NaCl Hydrogels**[a]

| ribbons | C (g cm$^{-3}$) | cac (g cm$^{-3}$) | $10^{-10}\Delta b_{vol}$ (cm/cm$^3$) | $R_c = (2\alpha)^{0.5}$ (Å) | $(Q^2I)_0$ | $n_L$ (mol Å$^{-1}$) | $n$ ($d_{rep}$ = 19 Å) (mol) | $b$ (Å) $b/a$ |
|---|---|---|---|---|---|---|---|---|
| NMM-DC | 0.0105 | ~0.0047 | −5.895 | 18.2 | 0.091538 | 0.094 | 1.8 | 18.5 < 0.1 |
| DABCO-DC | 0.0172 | ~0.0062 | −5.833 | 16.1 | 0.048219 | 0.088 | 1.7 | 18 .1 |

| cylinders | $C$ | cac (g cm$^{-3}$) | $10^{-10}\Delta b_{vol}$ (cm/cm$^3$) | | $(QI)_0$ (Å$^{-1}$ cm$^{-1}$) | $n_L$ (mol Å$^{-1}$) | $n$ ($d_{rep}$ = 4.5 Å) (mol) | |
|---|---|---|---|---|---|---|---|---|
| NMP-DC | 0.0095 | ~0.0015 | −5.977 | 56 | 0.509054 | 12.8 | 58 | 58 .7< $e$ <1 |

[a] The radius value $R$ is deduced assuming a plain, homogeneous cylindrical morphology. α is the slope of the linear part of a ln($QI$) versus $Q^2$ plot from which an "apparent" $R_c$ value is extracted. Critical aggregation concentrations (cac) were measured by following the fluorescence anisotropy of an 8-anilinonaphthalene sulfate (ANS) probe solubilized in the DC aggregates (Supporting Information).

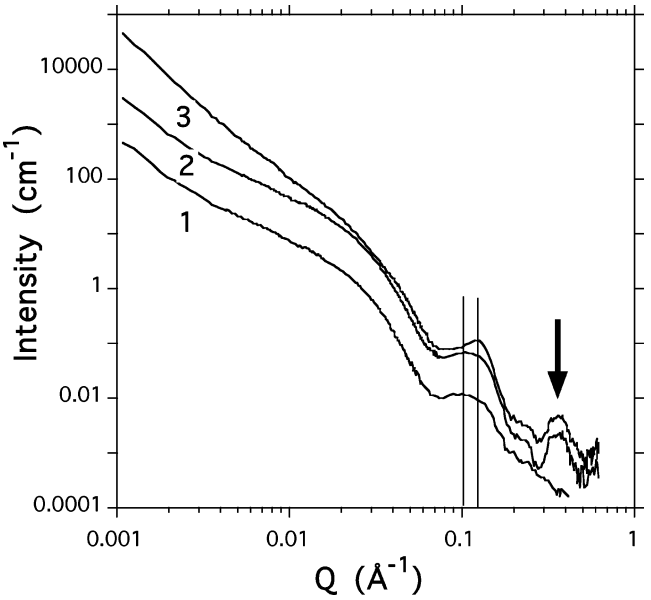


**Figure 3.** SANS profiles of NMP-DC gels at different concentrations (0.5 M NaCl): 1, $C$ = 0.00208 g cm$^{-3}$; 2, $C$ = 0.00946 g cm$^{-3}$; 3, $C$ = 0.0201 g cm$^{-3}$. A bold arrow points at a Bragg peak at 0.357 Å$^{-1}$. The two vertical bars indicate the shift of the apex of the first oscillation.

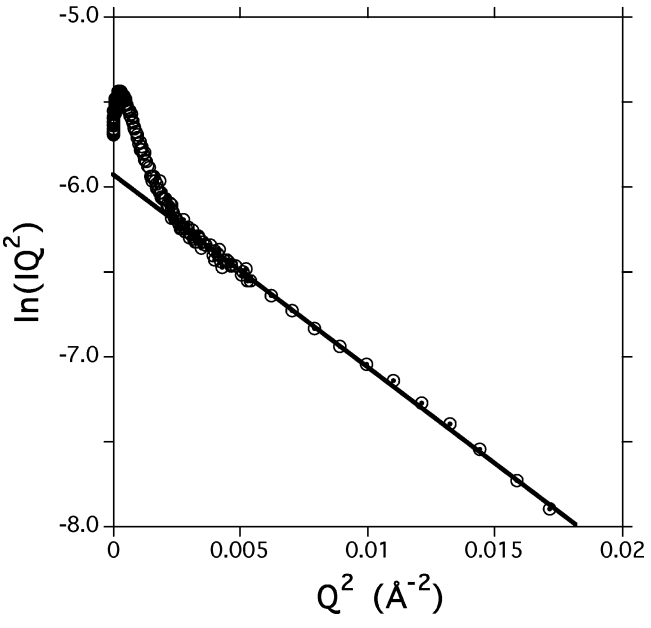


**Figure 4.** NMM-DC hydrogel ($C$ = 0.01052 g cm$^{-3}$, 0.5 M NaCl). Guinier plot for ribbonlike aggregates ($t$ = 36.9 Å; see text).

the Bragg peak at $Q$ = 0.371 Å$^{-1}$ ($\langle d \rangle$ = 16.9 Å) corresponds to reticular planes spaced by a molecular distance. A final confirmation of the ribbon structure will be obtained from the analysis of the absolute scattered intensities (vide infra and Table 1). Ribbons have a thickness built up with bilayered molecules, an architecture favored by the oxygen atom in the heterocyclic graft (Chart 1) in contrast to NMP-DC, which lacks such a terminating polar part and forms thicker and cylindrical fibers with no evidence for bilayered organization. The evolution of SANS curves with the NMM-DC concentration is only a gradual intensity shift along the ordinate axis proportional to the concentration (not shown), justifying the form-factor analysis in this concentration range.

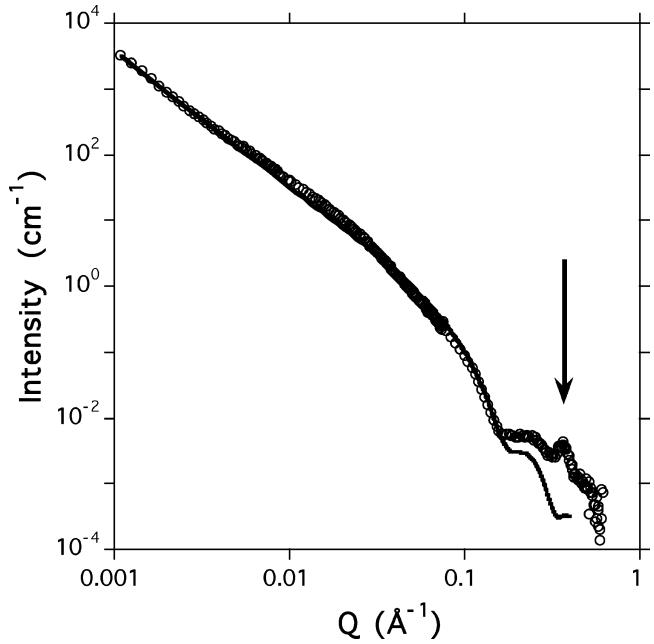


**Figure 5.** SANS of a NMM-DC hydrogels ($C$ = 0.0105 g cm$^{-3}$, 0.5 M NaCl, circles) and corresponding best theoretical fit (full line) for a ribbonlike morphology with elliptical sections: $b$ = 20 Å, ellipticity $b/a$ = 0.1. The arrow points at a Bragg peak at $Q \approx$ 0.371 Å$^{-1}$.

**DABCO-DC Hydrogels.** The DABCO-DC system exhibits a scattering curve similar to that for NMM-DC with the exception of the absence of a Bragg peak at this concentration (Figure 1). Figure 6 shows three examples of theoretical scattering curves approaching the experimental profile and chosen to present a common oscillation at 0.229 Å$^{-1}$ preceded by a similar sharp decay. Clearly, the cylindrical and lamellar morphologies (curves 1 and 2) cannot model the experimental scattering profile. The situation for ribbons with elliptical sections illustrates some interesting scattering specificities in the low $Q$ range. In particular, the decay before the oscillation can present a slight change of slope (in between the two vertical dotted bars) if the long side of the section 2$a$ is such that $Q_{min} < Q < 1/2a$, allowing the $Q^{-1}$ decay to be partly recovered (a plateau in Figure 6). Such a feature can be barely discerned in the experimental data. Curve 3 exhibits a significant departure in the low $Q$ part that suggests the presence of other morphol-

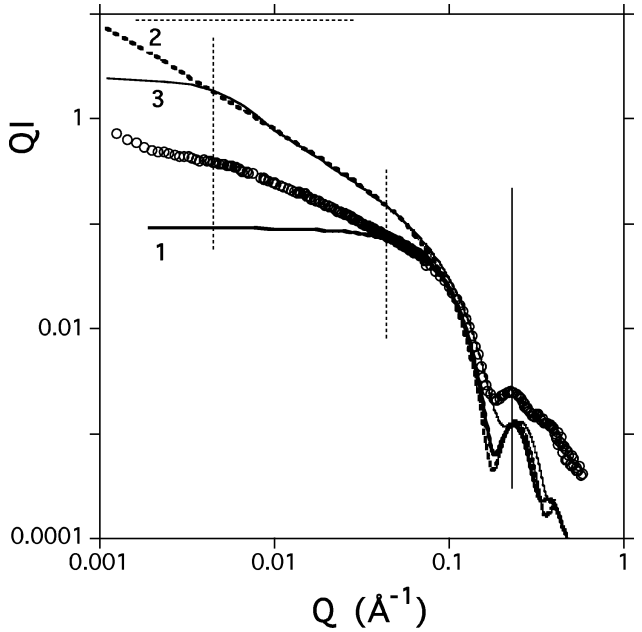


**Figure 6.** Cross-sectional intensity versus $Q$ of a DABCO-DC hydrogel (0.5 M NaCl) at $C = 0.0172$ g cm$^{-3}$ (open dots). Full lines are theoretical scattering for 1, a cylindrical morphology, $R = 22.8$ Å (as deduced from Figure 10), 2, a lamellar morphology, transverse thickness $t = 36$ Å, and 3, a ribbonlike morphology, ellipticity ratio of the sections $b/a \approx 0.1$ and half-thickness $b = 18$ Å.

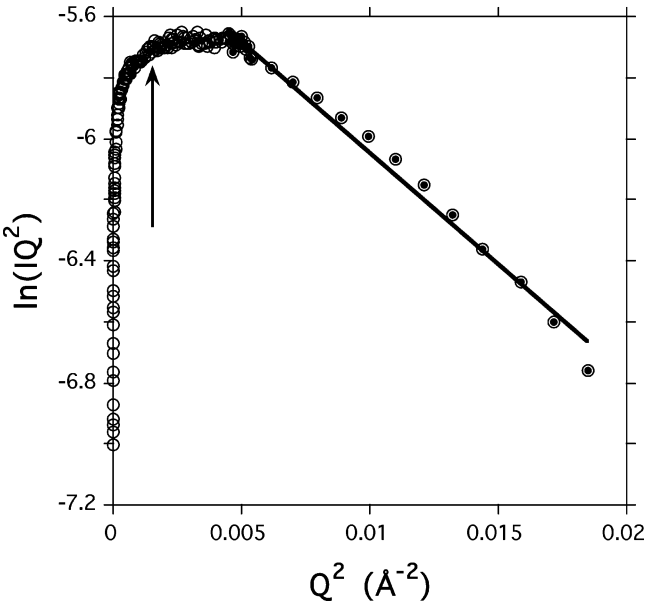


**Figure 7.** Determination of the transverse radius of gyration of lamellar-like scatterers in a DABCO-DC salted hydrogel (0.5 M NaCl) at $C = 0.0172$ g cm$^{-3}$. $R_t^2 = 72.7$ Å$^2$ corresponds to $t = 29.5$ Å ($R_t^2 = t^2/12$). The arrow points at the $Q$ value used for the estimation of the sectional size of the ribbon.

ogies, partly obscuring the native form-factor signal as will be further complemented with a concentration study (vide infra). A $\ln(Q^2I)$ versus $Q^2$ plot (Figure 7) appropriate for flattened ribbons shows three characteristic features. First, from the linear part, a transverse dimension $t = 29.5$ Å is extracted that is similar to the molecular length. Second, a plateau at lower angles confirms the lamellar-like character of the fibers. Third, the sharp decrease of the intensity at $Q \rightarrow 0$ is an indication of the finite size of the anisotropic sections. The arrow indicates the $Q$ limit of the crossover regimes ($Q^2 \approx 0.0015$ Å$^{-2}$), and the corresponding correlation distance ($\langle d \rangle \approx 160$ Å) indicates an

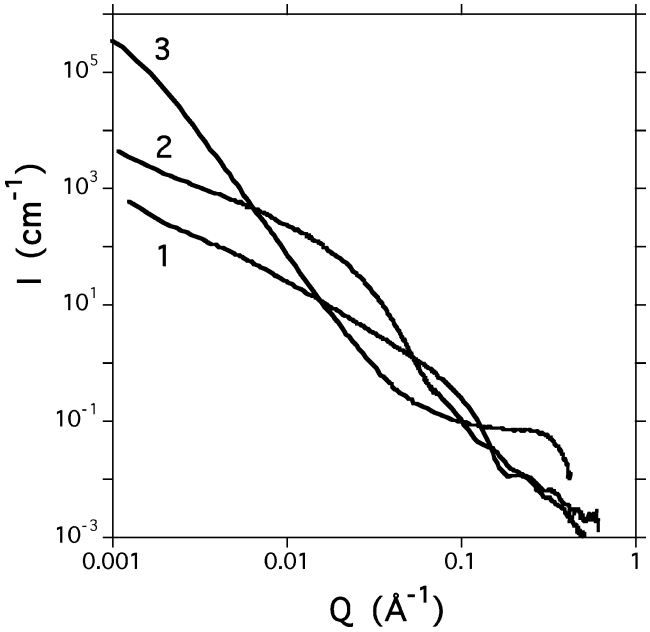


**Figure 8.** Variation of the cross-sectional intensity versus $Q$ profile versus the DABCO-DC concentration in salted hydrogels (0.5 M NaCl): 1, $C = 0.0172$ g cm$^{-3}$; 2, $C = 0.0336$ g cm$^{-3}$; 3, $C = 0.0496$ g cm$^{-3}$.

anisotropy of the section of ca. $29.5/160 \approx 0.18$ also supported by the value used for the fit of the experimental scattering curve.

In contrast to the two other DC systems, the variation of the scattering with DABCO-DC concentration is spectacular (Figure 8). The sharp decay in the intermediate $Q$ range, typical of finite-sized sections, occurs at much lower angles for a concentrated system while the asymptotic low $Q$ slope flattens from $-1.7$ to $-1.2$. This flattening was already distinguished with the former dilute gel (Figure 6) and indicated a more complex structural composition of the gel. For the concentrated gel of Figure 8, a good agreement is obtained with a fit using slightly anisotropic cross sections ($b/a \approx 0.6$) of the fibers ($b \approx 59$ Å) that describe both the position and amplitude of the two large $Q$ oscillations (two vertical bars in Figure 9). The $QI$ versus $Q$ representation highlights the change from a ribbonlike shape toward a more cylindrical and larger morphology since the low $Q$ $Q^{-1}$ plateau and the two oscillations can be clearly identified. Interestingly, the average diameter of the cylindrical resulting fibers (118 Å) is about 4 times the thickness of the original ribbons (29.5 Å). Considering the significant monodispersity of the cylindrical sections, supported by the presence of the two large $Q$ oscillations, it points at the existence of a specific aggregation mechanism. A weak Bragg peak is discerned at $Q = 0.329$ Å$^{-1}$ ($\langle d \rangle = 19.0$ Å) corresponding to diffraction planes separated by molecular distances. The DABCO-DC network appears less "crystalline" in comparison to NMM-DC and NMP-DC systems, whose diffraction peaks are more intense. If the concentration is still increased ($C = 0.0496$ g cm$^{-3}$), then the signal evolves toward a monotonic sharp $Q^{-4}$ decay (curve 3, Figure 8). Such a scattering profile can be accounted for assuming a random distribution of large-scale heterogeneities in the DABCO-DC network (Debye-Bueche's model, Supporting Information)[11] with a characteristic correlation distance $\langle \Xi \rangle \approx 1000$ Å. The process of merging of fibrils to ribbons can extend to even larger aggregates in a resulting crystalline SAFIN characterized by a scattering overwhelmed by a $Q^{-4}$ decay.

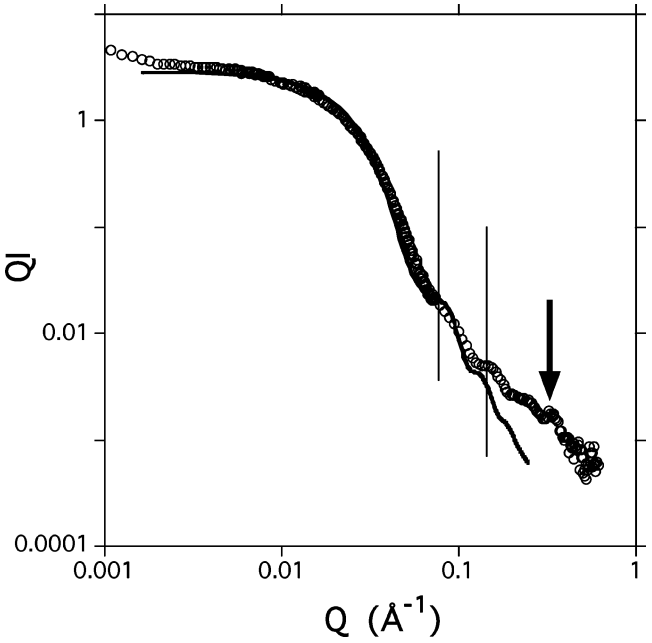


**Figure 9.** Best fit of the cross-sectional intensity versus $Q$ of a DABCO-DC hydrogel ($C = 0.0336$ g cm$^{-3}$, 0.5 M NaCl, open dots) with the theoretical scattering (full line) with fibers having a ribbonlike morphology ($b = 59$ Å, elliptical anisometry $b/a = 0.6$).

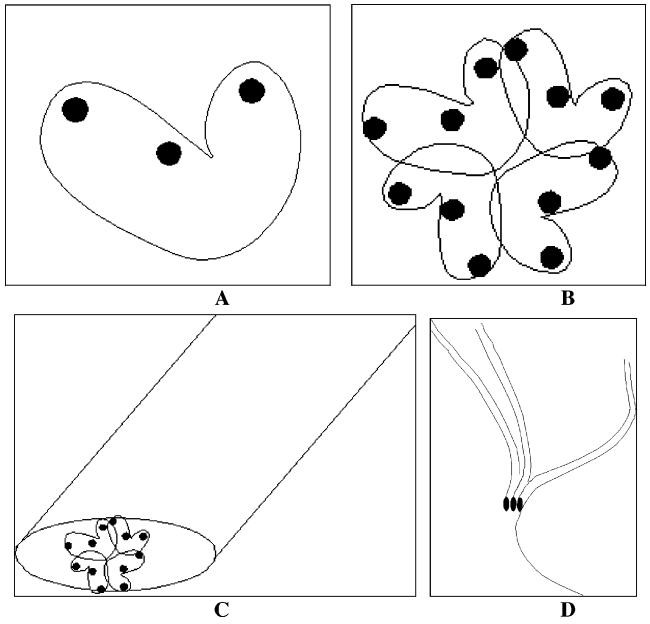


**Figure 10.** Naive scheme of the aggregation mechanism in DC systems. (A) Representation of the DC molecule. The facial amphiphilic steroid rings are represented as the sickle shapes. The dark full circles are polar centers (OH, $N^+$, or O) acting as connection sites. (B) One of the possible models of the cross-sectional aggregation mechanism. (C) Ribbon morphology. (D) Bundling mechanisms in DC-SAFINs.

## Discussion

The extraction of the number of aggregated molecules per unit length $n_L$ from the extrapolated intensity at $Q \rightarrow 0$ of the cross-sectional intensity (Supporting Information) is more delicate for ribbonlike structures but can still be used to support the analysis. The present data have shown that only one of the two dimensions of the sections, related to the molecular length, displays a significant monodispersity revealed by one or two intensity oscillations in the large $Q$ range. The dispersity attached to the large axis of the elliptical sections is large. To minimize the free energy of the assemblies, the curved hydrophobic DC steroid rings are hindered within structures further stabilized by electrostatic interactions between charged heterocyclic parts. Primary cross-sectional building blocks[12] are formed with pairs of associated molecules. Along the axial direction of the fibers or ribbons, hydrogen-bonded molecules infinitely stack (spacing distance of ca. 4−5 Å) to limit the end-cap energy costs. Additional secondary aggregation can also develop in certain conditions (e.g., an increase of concentration in the DABCO-DC system) to limit the energy costs due to the exposed edges of the primary ribbons. The concentration can thus trigger the formation of larger aggregates (bundling). For NMP-DC, the extrapolated absolute intensities $(QI)_0$ are considered in the context of cylindrical fibers to extract the number $n$ of molecules involved per cross-sectional repeating unit. With ribbonlike structures (NMM-DC and to a lesser extent DABCO-DC), the number of molecules $n$ involved in the transverse direction of the ribbons (Table 1) can be extracted from the $(Q^2I)_0$ values. $n \approx 2$ for NMM-DC and DABCO-DC, confirming the bimolecular association mechanism and is consistent with the SANS fits. For NMP-DC fibers, the number of aggregated molecules per unit length $n_L$ ($\ln(QI)$ versus $Q^2$ plot) is 12.8 mol.Å$^{-1}$ and corresponds to ∼58 molecules per sectional unit. Such value of $n_L$ (assuming a density of 1.1) corresponds to a section $A \approx 11\,075$ Å$^2$. For elliptical sections with $b = 58$ Å, as deduced from the fit of the scattering curve, a value of half of the long axis $a = 61$ Å can be estimated ($A = \pi ab$) that agrees with the above analysis, giving also a radius value of ca. 58 Å with a slight anisotropy of the sections.

The structures and behaviors of DC systems differ significantly in this series of systems. First, NMP-DC aggregates are fibers with slightly elliptical sections ($b = 58$ Å, $b/a = 0.7$). The gel state is characterized by a specific crystalline morphology (characteristic periodicity $\langle d \rangle \approx 50.7$ Å). Second, NMM-DC aggregates are flat ribbons having a bimolecular thicknesses and a $b/a$ ratio lower than 0.1. The concentration of gelator does not affect the average picture of the NMM-DC SAFINs. Third, DABCO-DC aggregates in salted gels are strikingly sensitive to the concentration of the gelator. A transition from ribbons ($b = 18$ Å, $b/a = 0.1$) to thicker and less anisometric fibers ($2b = 2 \times 59$ Å, $b/a = 0.6$) is observed upon a concentration increase. The three DC gels exhibit Bragg peaks at $Q \approx 0.33$ Å$^{-1}$ associated with the molecular length. Consistent with the previous rheological behaviors, the DC SAFINs appear crystalline-like and thus rigid. The amplitudes of the scattering peaks at similar concentrations are in the sequence NMP-DC > NMM-DC > DABCO-DC. A common feature of the DC systems is the propensity to form ribbonlike aggregates. A variety of dimensions and structural evolutions have been identified that underline the influence of small chemical modifications on the aggregation reactions in this class of SAFINs. These later do not concern the steroid core but the appended heterocycle and may transform the facial amphiphilic character of the deoxycholic acid derivative to a more classical surfactant. Interpenetrated molecular associations compose the building blocks characterized by a Bragg peak at a molecular distance. The monodispersity observed for one of the cross-sectional axes is related to the molecular length $l_{mol}$. The presence of hydroxy groups and oxo or nitroso parts favors the interdigitation of the molecules and are potential anchoring centers for connections. Figure 10 summarizes the situation at different length scales: the molecular level and the connection sites, the section of ribbons with molecules leading to a molecular or bimolecular characteristic transverse dimension,

the ribbons and the network with its zones where they merge into microcrystalline domains with diffracting planes spaced by multiples of the molecular length.

## Conclusion

Sodium deoxycholate aqueous solutions are known to exhibit different levels of molecular organization, and the aggregation reaction proceeds from primary[13−15] to secondary micelles.[12,16,17] The interaction between hydrophobic and hydrophilic surfaces favors the development of extensive hydrogen bonding between hydroxyl groups and side chain carboxylate anions. As a result, linear aggregates and bundles are generated from four-unit sodium deoxycholate primary micelles. Similarities of the X-ray scattering features in the diffraction patterns of aqueous solutions, gels, and crystals were used to propose a common type of helical structure developing with a ca. 21-Å diameter.[14,15] The aggregation behavior of water solutions of sodium cholate, deoxycholate, and chenodeoxycholate bile salts has also been investigated by small-angle X-ray measurements, and it was shown that micelles with uniform sizes are formed in the dilute range while an increase of concentration induces a micellar size growth. The scattering profiles are profoundly different from those observed for NMP-DC, NMM-DC, and DABCO-DC systems and are typical of interacting micelles with a scattering low $Q$ peak characterizing their arrangement.[18] Light-scattering measurements have also suggested the existence of a sphere-to-rod transition at high NaCl concentrations in sodium taurodeoxycholate solutions.[19] Also, mixtures (e.g., in the presence of vaccinia virus,[20] glycylglycine,[21,22] or glycine[23]) with sodium deoxycholate can produce thin helical strands.

DC systems have a cationic side chain replacing the anionic carboxylate group of the sodium deoxycholate derivative. The modification profoundly affects the aggregation properties. The present data show that in salted aqueous solutions linear aggregates form the networks involving bundlelike nodal zones and ribbons with anisotropic sections corresponding to multiples of the molecular length.

In an attempt to relate the structures in DC-SAFINs to the viscoelastic properties of their gels, it is observed that DC-SAFINs exhibit crystalline features (amplitude of the Bragg peak at large $Q$) in the sequence NMP-DC > NMM-DC > DABCO-DC. It is also the sequence of cross-sectional dimensions of the fibers as given by $R_c$ (Table 1). The elastic shear moduli of the gels follow the same order $G'_{NMP} > G'_{NMM} \approx G'_{DABCO}$.[3] Although the bending modulus of a single fiber $\kappa$ is known to increase by a power 4 with its section[24] through the Young modulus of the material, the transcription to a complex SAFIN is not trivial but should not modify the sequence. The scattering data are in this respect consistent with the rheological properties. This order is also that deduced from the size of the birefringent domains based on optical observations under crossed polarization.[3] Despite the fact that the DC gels appear optically anisotropic, the neutron-scattering patterns remain isotropic due to the averaging of numerous ordered domains of micron sizes over a square centimeter of the irradiated surface of the specimens. The sensitivity of the structures with the gelator concentration is striking for DABCO-DC; a remarkable ribbon to thick cylinder transition can be induced. The DC aggregates exhibit versatile "secondary" aggregation behaviors. Interestingly enough, the involvement of four DABCO-DC ribbons in cylindrical fibers observed at high concentrations can be considered as reminiscent of what is observed with classical deoxycholate solutions (vide supra). It is also intriguing to observe similarities with the mechanism of enhancement of fibril stability in solutions of twisted tapes made up of self-assembled peptides.[25] The formation of fibers from the chiral peptide tapes is attributed to intertape face-to-face attractions while their stabilization is due to their intrinsic chirality leading to intertwisting processes. A theory has been developed that predicts the monodispersity of the resulting fibers from the expression of an energetic balance involving the cost of the exposed edges of the ribbons and the energy gain due to the face-to-face attraction expressed using appropriate elastic components for the twist distortions. Such a context is likely applicable to a variety of systems from amyloid fibers to cellulose microfibrils and various chiral fibers found in SAFINs[26] including the DC systems. NMM-DC salted gels have a singular structural situation in that ribbons are a unique morphology forming their SAFINs. In comparison to the negatively charged deoxycholate solutions, the modified cationic DC bile salts thus exhibit different and original structural properties and behaviors.

**Acknowledgment.** The present work was supported by the Indo-French Center for Promotion of Advanced Research (IFCPAR project 2605-1), which is deeply thanked. The Institut Laue Langevin (Grenoble, France) is acknowledged for providing access to the spectrometer and all technical support.

**Supporting Information Available:** Critical aggregation concentrations, basic equations for small-angle scattering of fibrillar systems, and SANS of ribbons. This material is available free of charge via the Internet at http://pubs.acs.org.

## References and Notes

(1) Lipowitz, V.; Liebigs, A. *Ann. Chem. Pharm.* **1841**, *38*, 348.
(2) Terech, P. Small-Angle Scattering and Molecular Gels. In *Molecular Gels: Materials with Self-Assembled Fibrillar Networks*; Weiss, R. G., Terech, P., Eds.; Springer: New York, 2005.
(3) Sangeetha, N. M.; Bhat, S.; Maitra, U.; Terech, P. *J. Phys. Chem. B* **2004**, *108*, 16056.
(4) Kaplun, A.; Talmon, Y.; Konikoff, F. M.; Rubin, M.; Eitan, A.; Tadmor, M.; Lichtenberg, D. *FEBS Lett.* **1994**, *340*, 78.
(5) Terech, P.; de Geyer, A.; Struth, B.; Talmon, Y. *Adv. Mater.* **2002**, *14*, 495.
(6) Institut Laue-Langevin Homepage; http://www.ill.fr.
(7) Mittelbach, P.; Porod, G. *Acta Phys. Austriaca* **1961**, *14*, 405.
(8) Pedersen, J. S.; Schurtenberger, P. *J. Appl. Crystallogr.* **1996**, *29*, 646.
(9) Pedersen, J. S. *Adv. Colloid Interface Sci.* **1997**, *70*, 171.
(10) Glatter, O.; Kratky, O. *Small-Angle X-Ray Scattering*; Academic Press: London, 1982.
(11) Debye, P.; Bueche, A. M. *J. Appl. Phys.* **1949**, *20*, 518.
(12) O'Connor, C. J.; Wallace, R. G. *Adv. Colloid Interface Sci.* **1985**, *22*, 1.
(13) Bonincontro, A.; D'Archivio, A. A.; Galantini, L.; Giglio, E.; Punzo, F. *J. Phys. Chem. B* **1999**, *103*, 4986.
(14) Conte, G.; DiBlasi, R.; Giglio, E.; Paretta, A.; Pavel, N. V. *J. Phys. Chem.* **1984**, *88*, 5720.
(15) Esposito, G.; Giglio, E.; Pavel, N. V.; Zanobi, A. *J. Phys. Chem.* **1987**, *91*, 356.
(16) Mazer, N. A.; Carey, M. C.; Kwasnick, R. F.; Benedek, G. B. *Biochemistry* **1979**, *18*, 3064.
(17) Thomas, D. C.; Christian, S. D. *J. Colloid Interface Sci.* **1980**, *79*, 466.
(18) Zakrzewska, J.; Markovic, V.; Vucelic, D.; Feigin, L.; Dembo, A.; Mogilevsky, L. *J. Phys. Chem.* **1990**, *94*, 5078.
(19) Schurtenberger, P.; Mazer, N.; Känzig, W. *J. Phys. Chem.* **1983**, *87*, 308.
(20) McCrea, J. F.; Angerer, S. *Biochim. Biophys. Acta* **1960**, *42*, 355.
(21) Rich, A.; Blow, D. M. *Nature* **1958**, *46*, 423.
(22) Blow, D. M.; Rich, A. *J. Am. Chem. Soc.* **1960**, *82*, 3566.
(23) Campanelli, A. R.; De Sanctis, S. C.; Chiessi, E.; D'Alagni, M.; Giglio, E.; Scaramuzza, L. *J. Phys. Chem.* **1989**, *93*, 1536.
(24) Jones, J. L.; Marques, C. M. *J. Phys.* **1990**, *51*, 1113.
(25) Nyrkova, I. A.; Semenov, A. N.; Aggeli, A.; Boden, N. *Eur. Phys. J. B* **2000**, *17*, 481.
(26) Terech, P.; Weiss, R. G. *Chem. Rev.* **1997**, *97*, 3133.